Journal of Atmospheric and Solar–Terrestrial Physics 154 (2017) 47–54

Contents lists available at ScienceDirect

Journal of Atmospheric and Solar–Terrestrial Physics

journal homepage: www.elsevier.com/locate/jastp

Assessment of scintillation proxy maps for a scintillation study during geomagnetically quiet and disturbed conditions over Uganda

Emirant B. Amabayo[a,b,*], Edward Jurua[a], Pierre J. Cilliers[a,c]

[a] Department of Physics, Mbarara University of Science and Technology, P O Box 1410, Mbarara, Uganda
[b] Department of Physics, Busitema University, P O Box 256, Tororo, Uganda
[c] South African National Space Agency (SANSA) Space Science, P O Box 32, Hermanus 7200, South Africa

ARTICLE INFO

Keywords:
Low latitude scintillation
Scintillation proxies
Scintillation irregularities

ABSTRACT

The objective of this paper is demonstrate the validity and usefulness of scintillation proxies derived from IGS data, through its comparison with data from dedicated scintillation monitors and its application to GNSS scintillation patterns. The paper presents scintillation patterns developed by using data from the dedicated scintillation monitors of the scintillation network decision aid (SCINDA) network, and proxy maps derived from IGS GPS data for 2011 and 2012 over low latitude stations in Uganda. The amplitude and phase scintillation indicies (S_4 and σ_Φ) were obtained from the Novatel GSV4004B ionospheric scintillation and total electron content (*TEC*) monitor managed by SCINDA at Makerere (0.34^{0}N, 32.57^{0}E). The corresponding IGS GPS proxy data were obtained from the receivers at Entebbe (0.04^{0}N, 32.44^{0}E) and Mbarara (0.60^{0}S, 30.74^{0}E). The derived amplitude (S_{4p}) and phase (*sDPR*) scintillation proxy maps were compared with maps of S_4 and σ_Φ during geomagnetic storms (moderate and strong) and geomagnetically quiet conditions. The scintillation patterns using S_4 and σ_Φ and their respective proxies revealed similar diurnal and seasonal patterns of strong scintillation occurrence. The peaks of scintillation occurrence with mean values in the range $0.3 < (S_{4p}, sDPR) \leq 0.6$ were observed during nighttime (17:00–22:00 UT) and in the months of March-April and September-October. The results also indicate that high level scintillations occur during geomagnetically disturbed (moderate and strong) and quiet conditions over the Ugandan region. The results show that SCINDA and IGS based scintillation patterns reveal the same nighttime and seasonal occurrence of irregularities over Uganda irrespective of the geomagnetic conditions. Therefore, the amplitude and phase scintillation proxies presented here can be used to fill gaps in low-latitude data where there are no data available from dedicated scintillation receivers, irrespective of the geomagnetic conditions.

1. Introduction

The ionosphere is a partially ionised region of the Earth's atmosphere where incoming UV light ionises particles that form a layer from which radio waves can be reflected (Schunk and Nagy, 2009). The ionosphere crosses several meteorological layers and influences HF radio wave propagation to distant places on the Earth (McNamara, 1991). The ionosphere is a highly dispersive medium at Global Positioning System (GPS) frequencies. The electrical properties of this region allow it to transmit, reflect and refract radio waves as they traverse the ionosphere. Ionospheric plasma density sometimes gets distorted, making it turbulent and conducive for the development of ionospheric irregularities (Amabayo et al., 2014). Ionospheric irregularities manifest as enhancements or depletions of the electron density embedded in the ambient ionosphere (Davies, 1990; Amabayo et al., 2014). Since the ionosphere is dynamic, these irregularities are sometimes moving relative to the radio signals (Davies, 1990). The moving irregularities cause rapid, temporal fluctuations in the signal intensity and phase commonly referred to as amplitude and phase scintillation respectively (Davies, 1989; Amabayo et al., 2014).

Ionospheric scintillation predominantly occurs in the F layer and is known to have significant impact on radio communications, navigation and radar systems (Davies, 1990). Understanding the climatology of ionospheric scintillation both regionally and globally is essential to predict and mitigate the effects of scintillation on radio communication. Ionospheric scintillation pattern has been studied using data from dedicated scintillation receivers, such as the receivers in the scintillation network decision aid (SCINDA). The scintillation receivers have high installation and maintenance costs, making them unaffordable to many countries. However, scintillation in regions with insufficient

* Corresponding author at: Department of Physics, Busitema University, P O Box 256, Tororo, Uganda.
E-mail address: emirant.amabayo@gmail.com (E.B. Amabayo).

http://dx.doi.org/10.1016/j.jastp.2016.12.009
Received 30 May 2016; Received in revised form 12 November 2016; Accepted 23 December 2016
Available online 27 December 2016
1364-6826/ © 2016 Elsevier Ltd. All rights reserved.

scintillation monitors can now be studied using geodetic dual-frequency GPS receivers. Amplitude scintillation proxies derived from IGS station data by Amabayo et al. (2012) and phase scintillation proxies derived by Ghoddousi-Fard et al. (2013) have provided a good alternative for scintillation pattern studies in developing countries.

Low latitude scintillation has been of a great concern due to its prevalence and impact on the receiver tracking performance during the period of strong scintillation activity. Scintillation levels of (S_4, σ_Φ) ≥ 0.1 were considered by Amabayo et al. (2014). The study reported here was aimed at providing a scintillation proxy that can be used to fill gaps in SCINDA data that may hinder scintillation modelling over the African region. The scintillation proxy data was then used to develop scintillation patterns for two years (2011 and 2012), comparable with the SCINDA maps in Amabayo et al. (2014). A recent study by Tiwari et al. (2013) reported that ionospheric scintillation at low latitudes can either be inhibited or triggered during geomagnetic storms depending on the phase of the storm, its local time of occurrence and the location of the station. The study by Tiwari et al. (2013) showed that the occurrence of ionospheric scintillation observed during summer months was relatively weak compared to the occurrence recorded during winter and equinox months. According to Tiwari et al. (2013), enhanced magnetic activity suppresses the pre-midnight ionospheric scintillation during equinox and winter, while enhancement of pre-midnight scintillation activity was observed during summer months.

Perturbations induced by geomagnetic storms in the ionosphere have severe impacts on long distance communication and navigation systems. During geomagnetic storms, electron density perturbations may be positive (enhancement) or negative (depletion), which in turn influences the scintillation in different ways. According to Davies (1990), equatorial region scintillation occurs on magnetically quiet days and disappears with the onset of a magnetic storm. The same study stated that there is a strong correlation between scintillation and magnetic storm activity during autumnal and vernal equinoxes. The correlation is moderate during summer (near north solstice) and poor in winter. According to Buresova (2005), the storm effects in the F2 region of the ionosphere are predominantly attributed to ionospheric response to storm effects in the thermosphere. The effects in the lower ionosphere are predominantly caused by the storm-associated precipitation of energetic particles.

A study by Adewale et al. (2008) using GPS-derived *VTEC* observed at Libreville, Gabon (0.35°N, 9.67°E, dip lat 8.05°S), showed that during geomagnetic storms the altered electric fields contribute significantly to the occurrence of negative and positive ionospheric storm effects. The results revealed positive storm effects being more frequent than the negative storm effects. Positive storm effects generally last longer irrespective of the storm onset times. The same study observed that positive storm effects were more pronounced during daytime than the pre-midnight and post-midnight periods. A low latitude scintillation study conducted by Adewale et al. (2012) using scintillation data from Lagos (6.5°N, 3.4°E, mag lat 3.03°S), Nigeria, showed large scale *TEC* depletions, accompanied by increased rate of change of *TEC* (ROT) in the evening hours. This study also observed enhanced amplitude scintillation (S_4) associated with the *TEC* depletions and increased *ROT*. This observation led to a conclusion that plasma bubbles are associated with large scale irregularities (Adewale et al., 2012). The same study reported that the diurnal and seasonal scintillation percentage occurrence peaked during equinox months (March-April) at 23:00 LT. Similar results were obtained by Amabayo et al. (2014) in a scintillation pattern study over the Ugandan region.

In our study, disturbance storm time (Dst) index was used to investigate the relationship between geomagnetic storms and scintillation irregularities. This study adopted storm classification scheme by Tsurutani et al. (2006) and Loewe and Prölss (1997). The current study investigated only moderate (Dst ≤ −50 nT) strong (Dst ≤ −100 nT) and intense (Dst ≤ −200 nT) stroms (Loewe and Prölss, 1997; Tsurutani et al., 2006). Negative Dst values indicate the presence of a geomagnetic storm or sub-storm, and the more negative the Dst value, the higher the intensity of the storm. The decrease in the Dst index is the result of the storm time ring current which flows around the Earth from east to west in the equatorial plane. The ring current results from the differential gradient and curvature drifts of electrons and protons in the near Earth region and its strength is related to the solar wind conditions. Large magnetic storms with extreme Dst indices cause prompt penetration of the mid-latitude and equatorial ionosphere electric fields. This results in steep spatial *TEC* gradients and hence scintillation in GPS stations. Scintillation occurrence puts trans-ionospheric satellite communication and navigation at risk. Hence it is necessary to predict and correct errors associated with the phenomenon.

2. Data description and analysis

The raw GPS data were calibrated using the GPS_TEC algorithm developed by Gopi whose detailed description exists in Amabayo et al. (2012). Although GPS_TEC algorithm calculates *TEC* with an elevation mask of 20 °. For further analysis, an elevation cutoff of ≥30 ° was considered to filter multipath effects in the data. Standard geodetic dual frequency GPS data from the stations at Entebbe (EBBE) and Mbarara (MBAR) were used in this study to compute relative *TEC* from carrier-phase measurements. The *TEC* along the signal path between the receiver and the GPS satellite, commonly referred to as slant *TEC* (*STEC*) is defined by Eq. (1):

$$STEC = \int_R^S N_e ds, \tag{1}$$

where N_e is the electron density. The *TEC* is measured in *TEC* Units (TECU) with 1 TECU=10^{16} electrons/m^2, R and S stand for the receiver and satellite positions respectively. GPS satellites are observed along oblique signal paths which pierce the ionosphere at ionospheric pierce points (IPPs). The typical height of the IPP corresponds to the height associated with the peak electron density in the ionosphere, which is taken as 350 km for this study. The *TEC* along a vertical line through the IPP, commonly known as vertical *TEC* (*VTEC*) is modeled using a mapping function and the geographic position of the IPPs (Hoffmann-Wellenhof et al., 1992). Eq. (2) defines the mapping function used in this study.

$$VTEC = STEC \times \sqrt{1 - \left(\frac{R_E \times \sin(z_o)}{R_E + h_m}\right)^2} \tag{2}$$

where R_E and h_m are the mean radius of the Earth and the height of the ionosphere respectively, both measured in km, and z_o is the zenith angle (in degrees) at the observation site. For a known satellite position, z_o can then be calculated and the approximate coordinates of the IPP can be determined.

The *TEC* data was then used to derive the rate of change of *TEC* (*ROT*), rate of change of *TEC* index (*ROTI*) and from the *ROTI*, the S_4-proxy (S_{4p}). The S_{4p} was computed from *ROTI* by using an elevation-weighted coefficient (γ). The coefficient γ is calculated from a function of GPS satellite motion relative to the ionosphere, which is assumed to be concentrated on an imaginary thin shell 350 km above earth (the phase screen). The S_4 and S_{4p} were mapped to the zenith by using a mapping developed by Spogli et al. (2009). The *ROTI* and S_{4p} parameters were derived by means of Eqs. (3) and (4) respectively (Du et al., 2000).

$$ROTI = \sqrt{\langle ROT^2 \rangle - \langle ROT \rangle^2}, \tag{3}$$

$$S_{4p} = \gamma \times ROTI, \tag{4}$$

where the symbol ⟨⟩ in Eq. (3) implies average taken over 10 min and

$$\gamma = 6.2135 \times 10^{-3}\left[\frac{(v_p^2 + v_d^2 - 2v_p v_d \cos\alpha)\cos^3\varphi}{(r_S + h)\cos(\varphi + \theta)}\right],\ v_p = \frac{v_S(r_S + h)}{R_E + r_S},\ \varphi = \sin^{-1}\left[R_E \cos\left(\frac{\theta}{R_E + h}\right)\right],$$

with R_E the Earth radius (6378 km), h the assumed ionospheric height (350 km), θ the satellite elevation angle, α the GPS orbital plane inclination (55°), v_d the ion drift velocity (120 ms^{-1}) from Du et al. (2000), v_p the velocity of the IPP moving at h, v_S the satellite orbital speed (3874 ms^{-1}) and r_S the satellite orbital altitude (20,000 km). The elevation-weighted coefficient (γ) selectively suppresses low elevation scintillation compared to high elevation scintillation as shown in Fig. 1.

The phase scintillation proxy was derived using the approach of Ghoddousi-Fard et al. (2013) and Prikryl et al. (2013). According to Ghoddousi-Fard et al. (2013), the rate of change of ionospheric effects can be obtained from the delta phase rate (*DPR*) using the so-called geometry-free observables on carrier phase (ϕ_g) defined in Eq. (5)

$$\phi_g = L_1 - L_2 = \left(\frac{f_1^2}{f_2^2} - 1\right) I^s_{\phi_1,r} + (\lambda_1 N_1 - \lambda_2 N_2 + b_{\phi,r} + b^s_{\phi}) + \varepsilon_{\phi} \tag{5}$$

where f_1 and f_2 are the frequencies of the GPS signals, $I^s_{\phi_1}$ is the ionospheric effect on carrier phase at L_1 along the path between satellite s and receiver r, λ_1 and λ_2 are the wavelengths of the GPS signals, N_1 and N_2 are the integer ambiguities of the L_1 and L_2 GPS carrier phase measurements, $b_{\phi,r}$ and b^s_{ϕ} are receiver and satellite inter-frequency hardware delays on the carrier phase measurements respectively.

For two consecutive epochs (t_i and t_{i+1}) when there is no loss of lock, *DPR* can be computed using Eq. (6):

$$\psi = \frac{\varphi_g^{t_{i+1}} - \varphi^{t_i}}{t_{i+1} - t_i} = \frac{\left(\frac{f_1^2}{f_2^2} - 1\right) \times (I^{s(ti+1)}_{\phi_1,r} - I^{s(ti)}_{\phi_1,r})}{t_{i+1} - t_i} + \varepsilon_{\phi}. \tag{6}$$

where ε_{ϕ} is the combined multi-path and noise effects on delta phase rate and variations in receiver and satellite inter-frequency hardware delays over short intervals are assumed to be insignificant.

By assuming random noise and multipath over short intervals, a mean value ($<\psi_i>$) over a number of epochs can be derived to contain mainly the ionospheric disturbances. The mean delta phase rate (*mDPR*) and the standard deviation (*sDPR*) from the mean were derived using the expressions in Eqs. (7) and (8).

$$mDPR = <\psi_i> = \frac{\sum_{i=1}^{n} \psi_i}{n} \tag{7}$$

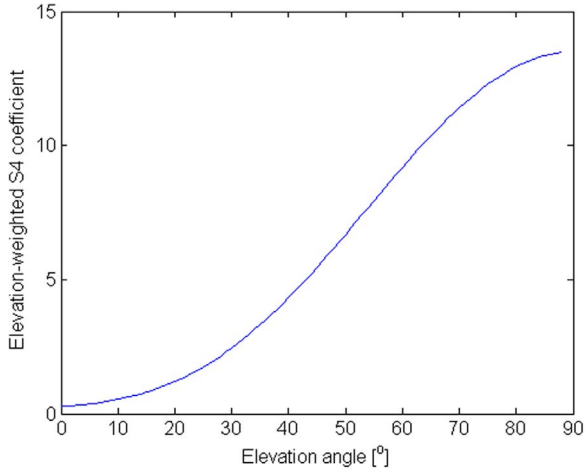


Fig. 1. Elevation weighting coefficient (γ) of Du et al. (2000) used to relate ROTI to the S4p.

$$sDPR = \sigma_{\psi} = \sqrt{\frac{1}{n}\sum_{i=1}^{n} (<\psi_i> - \psi_i)^2} \tag{8}$$

where n is the number of epochs used (e.g. 30 or 60 for 1 Hz GPS measurements). The *sDPR* was calculated over 10 min. Hence n=20 (for 30 s GPS data) and n=40 (for 15 s GPS data) to give a 10 min average in each case.

The absolute value of $<\psi_i>$ (|*mDPR*|) and σ_{ψ} (*sDPR*) were mapped to zenith to account for elevation angle of the signal path using the mapping function in the study by Spogli et al. (2009). Ghoddousi-Fard et al. (2013) stated that *sDPR* is better correlated with σ_{Φ} than *mDPR*, although both (*sDPR* and *mDPR*) correlate well with scintillation indices. Therefore, in this current study *sDPR* was considered for comparison with the standard σ_{Φ}. Prikryl et al. (2013) stated that *sDPR* does not capture the rapid changes of the phase in data sampled at 1 Hz, therefore, is not valid for strong scintillation. The *sDPR* and S_{4p} were scaled by factors of 0.035 and 10 to give values that match the σ_{Φ} and S_4 respectively. These scaling factors differ from those that apply to high latitudes. Scale factors were derived by selecting SCINDA and IGS datasets of a common time period. A correlation of the selected datasets was done and the root mean square (rms) values obtained for each SCINDA and scintillation proxy parameters derived from IGS data. The scale factors were then obtained by taking the ratio of rms value for SCINDA to the rms value for IGS data. The scaled proxy values were obtained by multiplying the raw proxies by the corresponding scale factors. The scaled proxy parameters were then used to develop the scintillation patterns.

3. Results and discussion

The amplitude (S_{4p}) and phase (*sDPR*) scintillation proxies derived in a study by Amabayo et al. (2015) were then used to develop scintillation patterns as presented in Fig. 2. The scintillation patterns based on scintillation proxies were developed in order to fill the data gaps in a climatology study by Amabayo et al. (2014). The scintillation patterns during selected geomagnetic storms and quiet periods are also presented in this study.

3.1. Scintillation pattern based on scintillation proxy

Amplitude and phase scintillation proxy (S_{4p} and *sDPR*) maps for the IGS station at Entebbe (EBBE) were developed for 2011 and 2012 using average scintillation values over a 10-min binning window. Hence n=20 (for 30 s GPS data) and n=40 (for 15 s GPS data) to give a 10 min average in each case. The bands of scintillation in Figs. 2a(i) and b(i) are due to multipath from fixed structures that cause scintillation from the same structures due to the same satellites approximately 4 min later every day due to the period of the GPS satellites being 11 h and 57.96 min, i.e. about 2 min less than 12 h per orbit and 4 min less than 24 h per day. The anomalous *sDPR* during December 2012 (Fig. 2d(ii)) is due to lack of data. The overall diurnal pattern reveals scintillation occurrence peaks between 17:00 and 22:00 UT (post-sunset). Strong scintillation values in the range 0.3–0.6 were observed during the months of March-April and September-October (Fig. 2). Fig. 2 shows that the diurnal and seasonal scintillation patterns for the IGS proxy scintillation patterns (Figs. 2b(i), b(ii), d(i) and d(ii)) are similar to those of SCINDA scintillation patterns obtained by Amabayo et al. (2014) (Figs. 1a(i), a(ii), c(i) and c(ii)). Hence the data gaps in the SCINDA (MAK) maps in Amabayo et al. (2014) can be filled with the IGS scintillation proxy data.. The diurnal and seasonal peak of scintillation ($0.3 < S_{4p}$, sDPR ≤ 0.6) occurs from 17:00 to 22:00 UT during the months of March-April and September-October. This scintillation proxy based study also reveals simultaneous occurrence of amplitude and phase scintillation over the region (Amabayo et al., 2014). A recent scintillation study by Olwendo et al. (2013) revealed occurrence during the post-sunset hours of the equinox months being more frequent than at the solstices. The post-sunset peaks observed in this current study

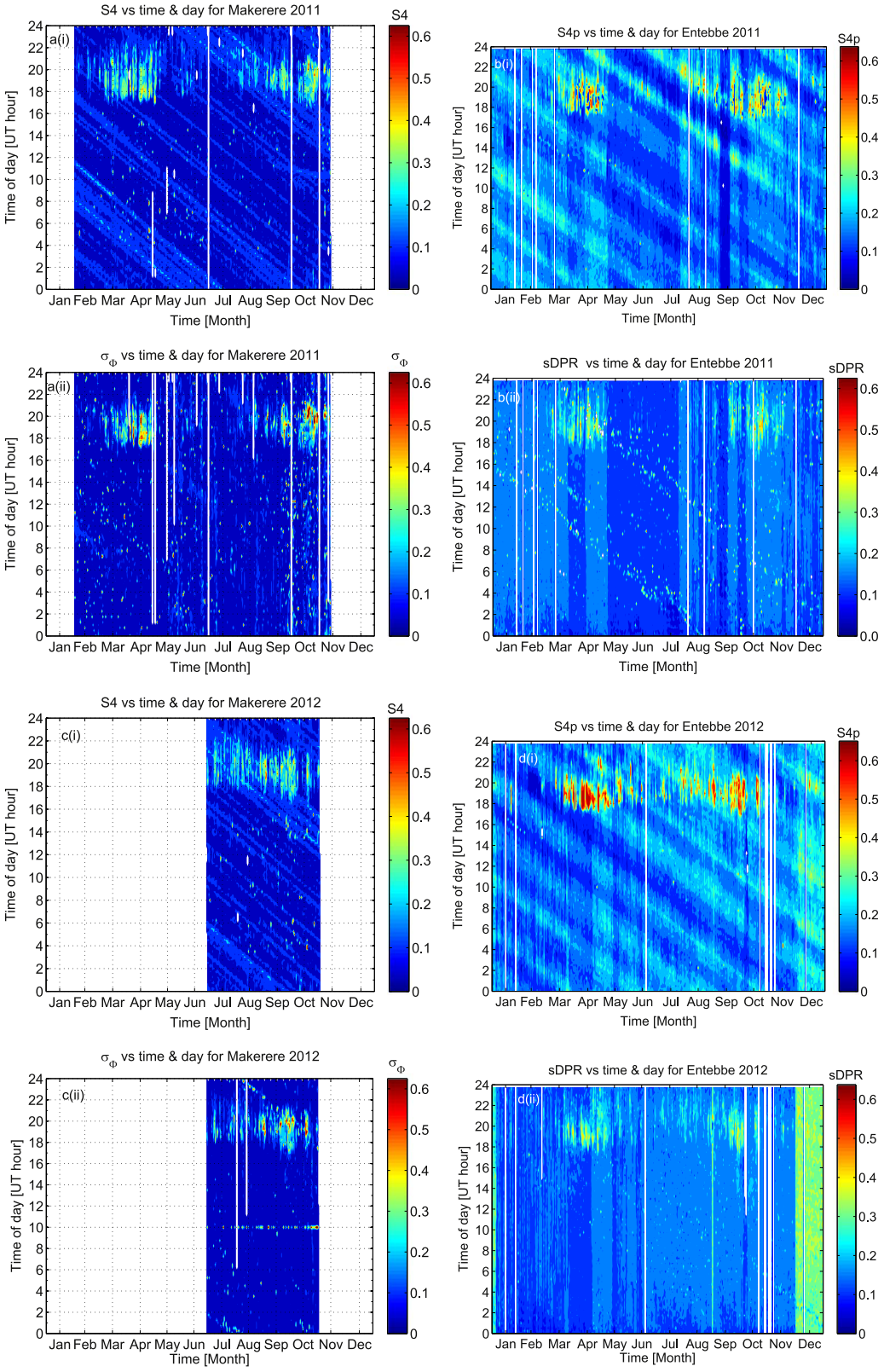


Fig. 2. Scintillation proxy pattern for the amplitude (a(i), b(i), c(i) and d(i)) and phase (a(ii), b(ii), c(ii) and d(ii)) scintillation for 2011 and 2012. Figures a(i), a(ii), c(i) and c(ii) were adapted from a paper by Amabayo et al. (2014).

are most likely associated with the equatorial plasma bubbles (EPBs) and wave-like structures observed by Amabayo et al. (2014, 2015) and by Paznukhov et al. (2012).

To further investigate the performance of the proxies, strong and moderate storm events were analysed to investigate cases of occurrence of ionospheric scintillation during geomagnetic storms. The aim here is to assess the proxy based climatology results during strong or moderate geomagnetic storms and during geomagnetically quiet periods. The results are presented in Figs. 4 and 5.

3.2. Scintillation maps for geomagnetically disturbed periods

Figs. 3a(iii) and b(iii) show the occurrence of moderate and strong storms from about 06:00 UT to 12:00 UT (06–07 April 2011) and 18:00 to 12:00 UT (24–25 October 2011) respectively. The storms were initiated by arrival of shock waves at the magnetosphere. The shock waves arrived at about 06:00 UT (Fig. 3a(i)) and 18:00 UT (Fig. 3b(i)) since the IMF Bz component turned southwards at these times. The main and recovery phases of the storms were accompanied by an increase and decrease of ion number density respectively. Geomagnetic storms result from a major disturbance of the magnetosphere that occurs when the heliospheric magnetic field (particularly Bz) turns southward and remains southward for a prolonged period of time. Geomagnetic storms occur in conjunction with ionospheric storms and can be caused by solar flares or high speed solar wind streams, which emanate from coronal holes. However, a geomagnetic storm resulting from a solar flare usually starts with the sudden commencement as an initial phase during which there is an increase in the intensity of the Earth's geomagnetic field, followed by a large decrease termed the main phase, and finally the recovery phase with possible sub-storms. These result in a significant variation in electron density in the ionosphere, and a simultaneous increase in absorption of radio waves. The variation in absorption of radio waves may manifest as ionospheric amplitude scintillation.

To assess the performance of the proxies during ionospheric scintillation and geomagnetic storms conditions, scintillation patterns during storm periods were plotted and compared. The results based on standard scintillation indices and their corresponding proxies were compared. In this study, geomagnetically quiet (super solar quiet) days (28–29 October 2011) which correspond to average Kp index +0 were considered. In addition, days (26–28 April 2011) with very low Kp values after the storm of 03–09 April 2011 were also considered. The proxy maps for these two cases were compared with maps obtained using scintillation indicies from SCINDA and results are presented in Fig. 4.

Figs. 4a(i) and b(i) show the occurrence of strong amplitude scintillation as observed by means of SCINDA S_4 and IGS derived S_{4p} proxy during moderate storm conditions. Figs. 4a(ii) and b(ii) show the occurrence of strong phase scintillation during the same moderate storm using the SCINDA σ_Φ and the IGS derived *sDPR* proxy. Strong amplitude and phase scintillation proxy levels in the range of 0.3–0.6 can be observed on 03, 04, 07 and 08 April 2011 between 18:00 UT and 23:00 UT. Thin patches of amplitude (Fig. 4a(i)) and phase (Figs. 4a(ii)) scintillation levels higher than 0.4 can be observed between about 04:00 UT and 12:00 UT. Strong amplitude and phase scintillation levels (>0.3) can be seen in Fig. 4c(i) and d(i) and c(ii) and d(ii) respectively. The scintillation patterns in Figs. 4c(i), c(ii) and d(i) and d(ii) reveals a clear band of post-sunset scintillation between 17:00 UT and 22:00 UT. The occurrence of strong scintillation in Figs. 4b(i) and b(ii) on 04 April 2011 and 08 April 2011 between 18:00 UT and 21:00 UT were observed on geomagnetically quiet days. Much stronger phase scintillation (σ_Φ and *sDPR*) levels were observed during the moderate and strong geomagnetic storms than the amplitude scintillation (S_4 and S_{4p}) during the same period between 17:00 UT and 22:00 UT. The occurrence of strong scintillation between 17:00 and 22:00 UT (20:00–01:00 LT) is most likely associated with the EPBs and wave-like structures that may induce travelling ionospheric disturbances (TIDs) (Amabayo et al., 2014).

3.3. Scintillation maps for geomagnetically quiet period

In this part of the study, geomagnetically quiet days correspond to the super solar quiet days (SSQ). The SSQ days chosen correspond to average Kp index +0 (28–29 October 2011). These days followed the storm of 24–27 October 2011. In addition, days (26–28 April 2011) with very low Kp values after the storm of 03–09 April 2011 were used to check the performance of the scintillation proxies during weak storm periods. The proxy maps were compared with maps obtained using scintillation indicies from SCINDA. The results are presented in Fig. 5.

Figs. 5a(i) and a(ii) show patches of high amplitude and phase scintillation levels (0.3–0.6) from 26 to 27 April 2011 during the night (17:00 UT-22:00 UT). The corresponding proxy maps in Figs. 5b(i) and b(ii) also reveal similar patches of high level scintillation on the same days from 17:00 UT to 22:00 UT. Figs. 5a(i), 5b(i) a(ii) and b(ii) show that amplitude scintillation was more dominant and stronger than phase scintillation over the region of study. The scintillation pattern revealed by the proxy maps in Figs. 5d(i) and d(ii) correlate very well with the pattern in Figs. 5c(i) and c(ii) between 18:00 UT and 21:00 UT. A clear band of nighttime scintillation occurrence was observed using both the proxy and SCINDA data at around 20:00 UT, despite loss of SCINDA data on 29 October 2011. The major motivation of this study lies in the data loss and how to compensate for it. The results in Figs. 5 indicate that both high and low level scintillations occur during geomagnetically quiet days over the low-latitude Ugandan region. Scintillation climatology studies by Ghoddousi-Fard et al. (2013) found that the location and time of occurrence of larger mean *DPR* (*mDPR*) values were similar for both geomagnetically disturbed and quiet periods in high-latitudes. At low-latitudes, both strong amplitude and phase scintillations can occur during SSQ days and weak storm periods. It has already been established that EPBs and wave-like structures or TIDs are responsible for the amplitude and phase scintillations over the Ugandan region (Amabayo et al., 2015, 2014; Paznukhov et al., 2012). High latitude studies by Ghoddousi-Fard et al. (2013) concluded that 1-second GPS phase differences averaged over 30–60 s is a useful proxy for phase scintillation. However, our current study shows that low-latitude 15-second and 30-second phase differences averaged over

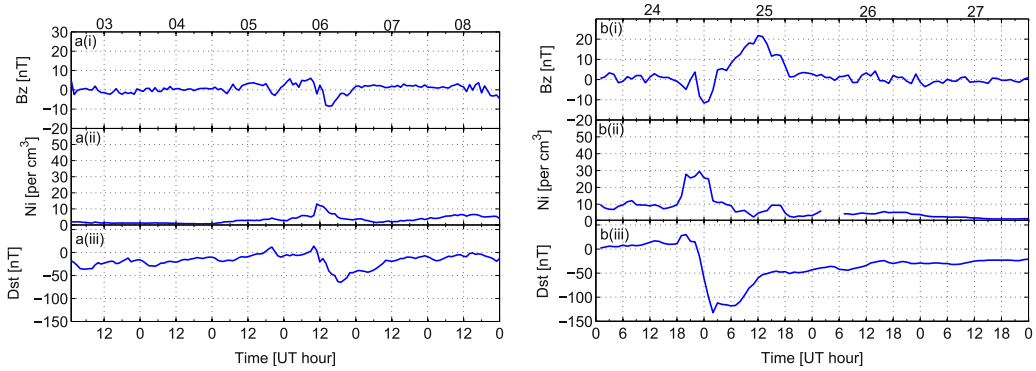


Fig. 3. Variability of the IMF (Bz) component (a(i) and b(i)), ion number density (a(ii) and b(ii)) and Dst index (a(iii) and b(iii)) for the geomagnetically disturbed periods 03–08 April 2011 and 24–27 October 2011 respectively. Dst data, solar wind and interplanetary magnetic field data was downloaded from the Coordinated Data Analysis Website (CDAWeb) of the Advanced Composition Explorer (ACE) satellite (http://cdaweb.gsfc.nasa.gov/cdaweb/sp_phys).

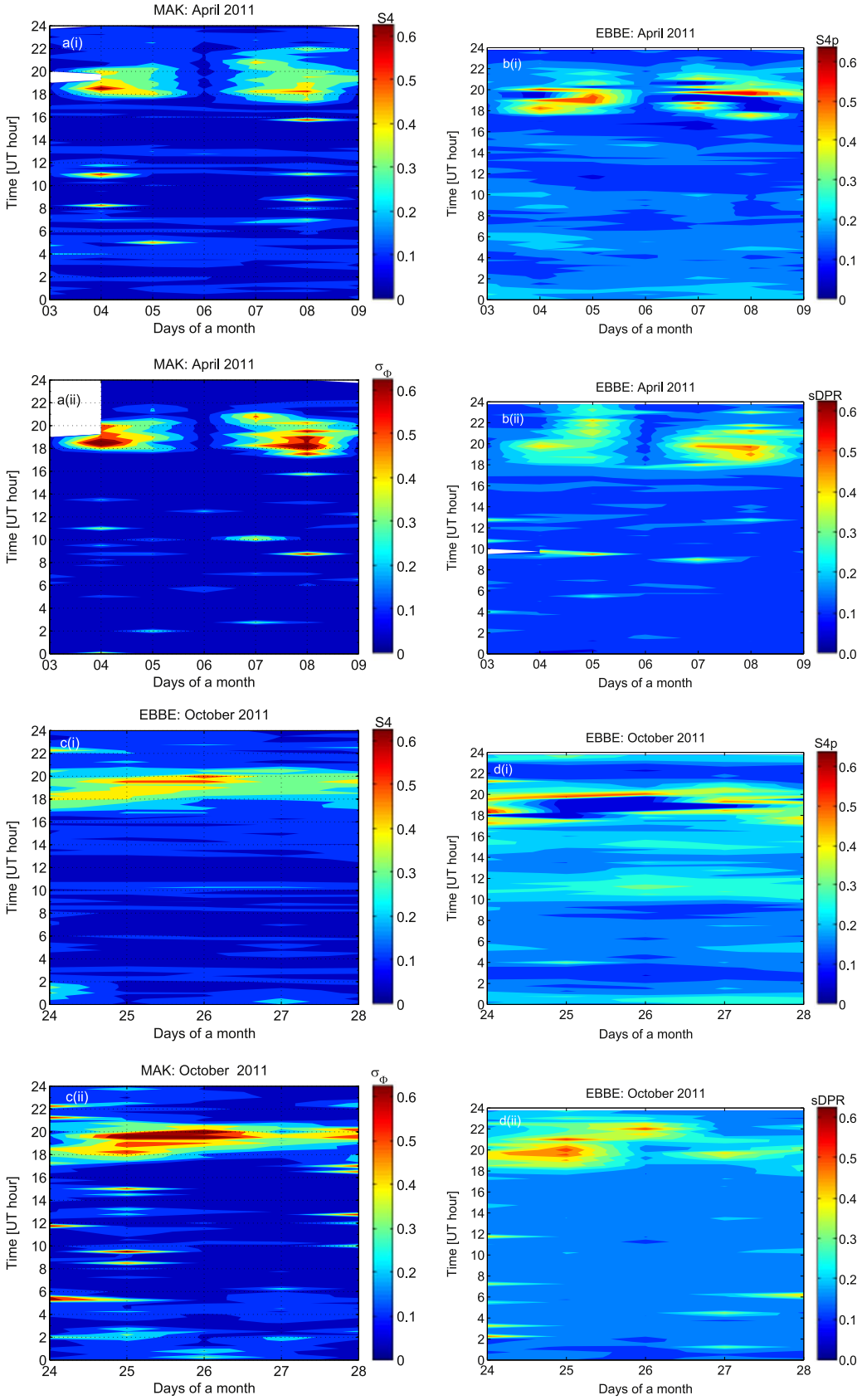


Fig. 4. Scintillation pattern S_4 and S_{4p}, σ_Φ and *sDPR* showing the diurnal occurrence of amplitude (a(i) and c(i)) and phase (a(ii) and b(ii)) scintillation during moderate (03–08 April 2011) and strong (24–27 October 2011) storms, respectively.

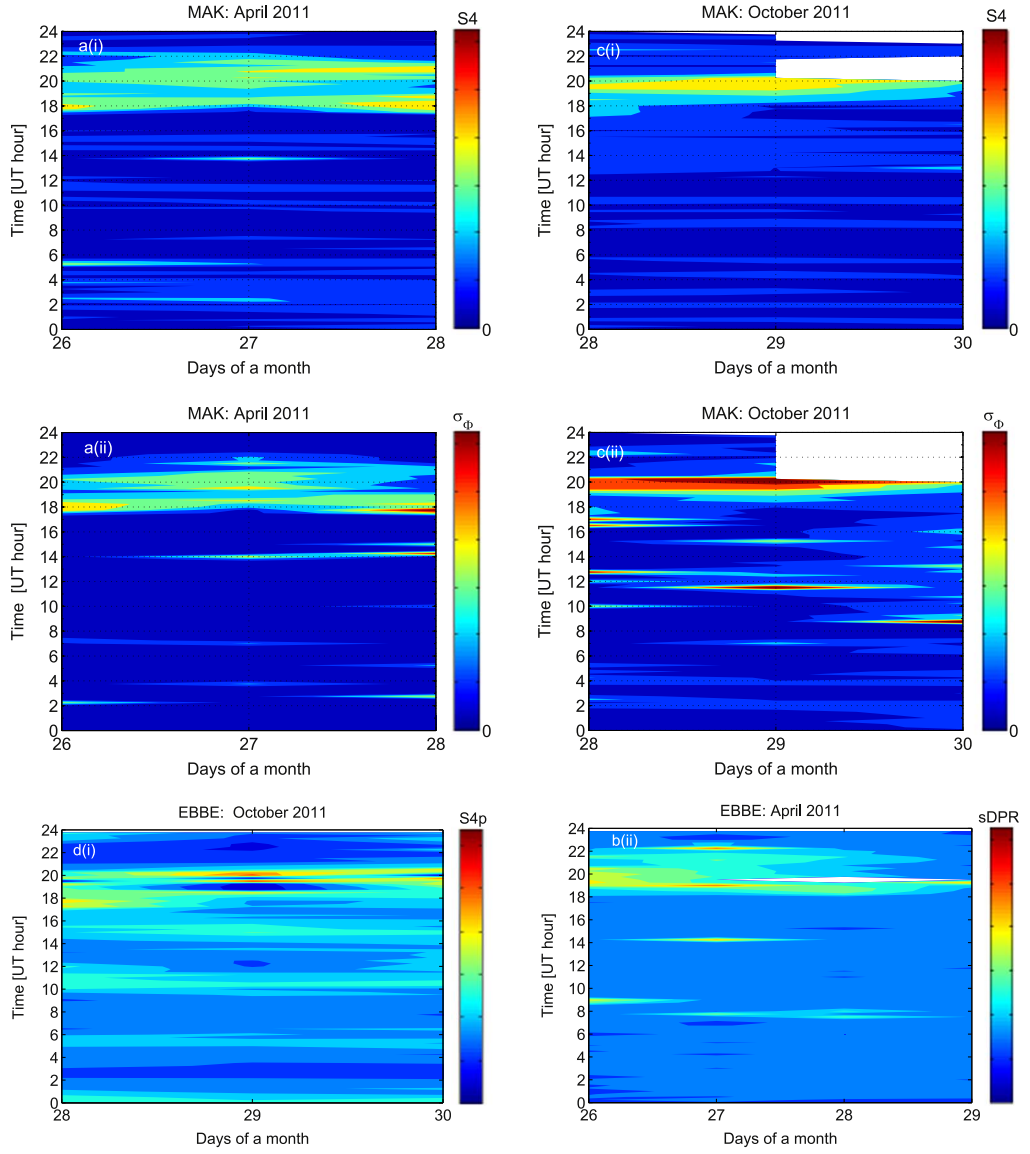


Fig. 5. Scintillation pattern for amplitude (a(i), c(i)) and phase (a(ii), c(ii)) scintillation using data from MAK (SCINDA). The corresponding amplitude (b(i), d(i)) and phase (b(ii), d(ii)) scintillation proxy pattern used data from EBBE (IGS) station. These patterns are for geomagnetically quiet periods.

1-min can serve as a good proxy for phase scintillation. The corresponding amplitude scintillation proxy also provides a good estimate of SCINDA based scintillation measurements at a station within 229 km. The distance between the IGS GPS stations at Entebbe (EBBE) and Mbarara (MBAR) from the SCINDA at Makerere (MAK) are 36.4 km and 229 km respectively.

4. Conclusion

The scintillation proxy maps developed using average scintillation values over a 10-min binning window show occurrence of amplitude and phase scintillation over the Ugandan region. The diurnal and seasonal peak of scintillation are observed between 17:00 UT and 22:00 UT and in the months of March-April and September-October respectively, similar to those obtained by Amabayo et al. (2014). Stronger phase scintillation (σ_Φ and *sDPR*) levels were observed during moderate and strong storms than amplitude scintillation (S_4 and S_{4p}) during the same period (17:00 UT and 22:00 UT). The results indicate that both high ($0.3 < S_{4p}$, $sDPR \leq 0.6$) and low level scintillations ($0.1 \leq S_{4p}$, $sDPR \leq 0.3$) occur during geomagnetically quiet days over the low latitude Ugandan region. Scintillation climatology studies by Ghoddousi-Fard et al. (2013) found that the location and time of occurrence of larger mean *DPR* (*mDPR*) values were similar for both geomagnetically disturbed and quiet periods. The scintillation characteristics obtained in this study are consistent with those observed by Ghoddousi-Fard et al. (2013) and Davies (1990).

At low latitudes, both strong amplitude and phase scintillations occur during either SSQ periods or weak storm periods. The occurrence of strong scintillation between 17:00 and 22:00 UT (20:00–01:00 LT) are most likely associated with the EPBs and wave-like structures that may induce TIDs (Amabayo et al., 2015, 2014; Paznukhov et al., 2012). Therefore, in this study, low latitude plasma irregularities have been captured very well during geomagnetically disturbed and quiet conditions using the amplitude and phase scintillation proxies. The results also show that scintillation data from SCINDA and IGS based proxies are in good agreement during geomagnetically disturbed and quiet conditions. Hence SCINDA data gaps such as those in Amabayo et al. (2014) can be filled with the IGS scintillation proxy data. This allows the extension of scintillation proxies to map irregularities that cause low latitude scintillation in locations where there are no scintillation receivers.

Acknowledgement

The authors acknowledge the International Science Program (ISP) from Uppsala University in Sweden for funding this study. We extent our appreciation to the Boston College and the Air Force Research Laboratory (AFRL), USA, for supplying the SCINDA receivers to Uganda. We also acknowledge the offer of IGS data used in this study, downloaded from ftp://data-out.unavco.org/pub/rinex/obs. We also acknowledge the management of Coordinated Data Analysis Website (CDAWeb) for online offer of Advanced Composition Explorer (ACE) satellite Dst data, solar wind and interplanetary magnetic field data.

References

Adewale, A.O., Oyeyemi, E.O., Adeloye, A.B., Ngwira, C.M., Athieno, R., 2008. Responses of equatorial F region to different geomagnetic storms observed by GPS in the African sector. J. Geophys. Res. 116, A12319. http://dx.doi.org/10.1029/2011JA016998.

Adewale, A.O., Oyeyemi, E.O., Adeloye, A.B., Mitchell, C.N., Rose, J.A.R., Cilliers, P.J., 2012. A study of L-band scintillations and total electron content at an equatorial station, Lagos, Nigeria. Radio Sci. 47, RS2011. http://dx.doi.org/10.1029/2011RS004846.

Amabayo, E., Jurua, E., Cilliers, P., Habarulema, J.B., 2014. Climatology of ionospheric scintillations and TEC trend over the Ugandan region. Adv. Space Res. 53, 734–743.

Amabayo, E.B., Jurua, E., Cilliers, P.J., 2015. Validating the use of scintillation proxies to study ionospheric scintillation over the Ugandan region. J. Atmos. Sol.-Terr. Phys. 128, 84–91.

Amabayo, E.B., McKinnell, L.A., Cilliers, P.J., 2012. Ionospheric response over South Africa to the geomagnetic storm of 11–13 April 2001, Journal of Atmospheric and Solar-Terrestrial Physics, 84-85 , pp. 62–74.

Buresova, D., 2005. Effects of geomagnetic storms on the bottom side ionospheric F region. Adv. Space Res. 35, 429–439.

Davies, K., 1989. Ionospheric Radio. Run Press, United Kingdom, (ISBN 0 86341 186 X).

Davies, K., 1990. Ionospheric Radio. Peter Peregrinus, London.

Du, J., Caruana, J., Wilkinson, P., Thomas, R., Cervera, M., 2000. Determination of equatorial ionospheric scintillation S4 dual frequency GPS, WARS'00, URSI Commission G, Workshop, La Trobe University, Australia.

Ghoddousi-Fard, R., Prikryl, P., Luhaye, F., 2013. GPS phase difference variation statistics: a comparison between phase scintillation index and proxy indices. Adv. Space Res. 52, 1397–1405.

Hoffmann-Wellenhof, B., Lichtenegger, H., Collins, J., 1992. Global Positioning System Theory and Practice. Springer-Verlag, Wien New York.

Loewe, C.A., Prölss, G.W., 1997. Classification and mean behavior of magnetics storms. J. Geophys. Res. 102, 209–213.

McNamara, L.F., 1991. The Ionosphere: Communications, Surveillance, And Direction Finding, Malabar, FL, Krieger.

Olwendo, O., Baluku, T., Baki, P., Cilliers, P., Mito, C., Doherty, P., 2013. Low latitude ionospheric scintillation and zonal irregularity drifts observed with GPS-SCINDA system and closely spaced VHF receivers in Kenya. Adv. Space Res. 51, 1715–1726.

Paznukhov, V.V., Carrano, C.S., Doherty, P.H., Groves, K.M., Caton, R.G., Valladares, C.E., Seemala, G.K., Bridgwood, C.T., Adeniyi, J., Amaeshi, L.L.N., Damtie, B., DUjanga, F.M., Ndeda, J.O.H., Baki, P., Obrou, O.K., Okere, B., Tsidu, G.M., 2012. Equatorial plasma bubbles and L-band scintillations in Africa during solar minimum. Ann. Geophys. 30, 675–682.

Prikryl, P., Ghoddousi-Fard, R., Kunduri, B.S.R., Thomas, E.G., Coster, A.J., Jayachandran, P.T., Spanswick, E., Danskin, D.W., 2013. GPS phase scintillation and proxy index at high latitudes during moderate geomagnetic storm. Ann. Geophys. 31, 805–816.

Schunk, R., Nagy, A., 2009. Ionospheres: Physics, Plasma Physics, and Chemistry, Cambridge Atmospheric and Space Science Series. Cambridge University Press, (ISBN 9780521877060).

Spogli, L., Alfonsi, L., Franceschi, G.D., Romano, V., Aquino, M.H.O., Dodson, A., 2009. Climatology of GPS ionospheric scintillations over high and mid-latitude European regions. Ann. Geophys. 27, 3429–3437.

Tiwari, S., Sarkar, S., Vishwakarma, A., Gwal, A.K., 2013. Effect of magnetic activity on scintillation at equatorial region during low solar activity. Adv. Phys. Theor. Appl. 19, 122–129.

Tsurutani, B.T., McPherron, R.L., Gonzalez, W.D., Lu, G., Gopalswamy, N., Guarnieri, F.L., 2006. Recurrent Magnetic Storms: Corotating Solar Wind Streams second edition. American Geophysical Union, Washington, D.C.